SrCo0.85Fe0.15O2.62 -Oxygen deficient "314-type" perovskite; a highly efficient cathode for solid oxide fuel cells

Sourav Marik, Clément Nicollet, Madhu Channabasappa, Sébastien Fourcade, Alain Wattiaux, Mathieu Duttine, Rodolphe Decourt, Jean-Marc. Bassat, Olivier Toulemonde

$SrCo_{0.85}Fe_{0.15}O_{2.62}$ - Oxygen deficient "314-type" perovskite; a highly efficient cathode for solid oxide fuel cells

Marik S.[a], Nicollet C.[a], Channabasappa M.[a], Fourcade S.[a], Wattiaux A.[a], Duttine M.[a], Decourt R.[a], Bassat J.-M.[a], Toulemonde O.[a]

[a]CNRS, Univ Bordeaux, ICMCB, UPR 9048, F 33600 Pessac, France

Supplementary materials on the editor web site

Abstract :

Structure, electrical conductivity and electrochemical performance for a new oxygen deficient perovskite material with composition $SrCo_{0.85}Fe_{0.15}O_{2.62}$ is explored here. It crystallizes in a "314-type" oxygen-vacancy ordered structure (Space Group: *I4/mmm*) with $2a_p \times 2a_p \times 4a_p$ unit cell, and contains alternate oxygen replete [Co2/Fe2-O] and oxygen deficient [Co1/Fe1-O] planes along c-direction. Room temperature Mössbauer spectroscopy and room temperature neutron powder diffraction confirm the presence of mixed valence states (3+ and 4+) for both Fe and Co. Polaronic behavior in the electrical conductivity is observed below 400 °C, and attributed to the presence of Co^{4+} and Fe^{3+} cations in the structure. The electrical conductivity at 600 °C is high enough (~200 S cm^{-1}) to act as a cathode material. At the same time, the polarization resistance measurements show an excellent value of 0.1 Ω cm^2 at 600 °C. These results suggest that at 600 °C, this material is a mixed oxide-ion and electronic conductor exhibiting excellent activity for the oxygen reduction reaction, making it a promising cathode material for an intermediate temperature solid oxide fuel cell.

1 Introduction

Solid oxide fuel cell (SOFC) has attracted much interest in recent years, due to their great potential for power generation related to our increasing need for sustainable energy resources [1]. A drive to reduce the operating temperature of the electrochemical cells to intermediate values (550–800 °C) is a prime target to increase durability and be cost effective. However, the electrode activity toward the oxygen reduction reaction (ORR) is limited by thermally activated parameters, such as oxygen-ion diffusion and oxygen surface exchange [2]. Thus, lowering the operating temperature results in a significant decrease of the electrode performance. To be efficient, an oxygen electrode has to be mixed electronic and ionic conductive. There are two ways to achieve this mixed conductivity: (i) either using a composite electrode [3] or (ii) searching for materials that possesses both conductivities, so called MIEC (for mixed ionic and electronic conductors). In recent years, much efforts have been spent exploring new MIEC materials that can work efficiently at intermediate or low temperature range [4].

Cobalt (Co) containing oxygen deficient, perovskite related oxides prompted great interest as MIEC oxides. Indeed, these are very important materials as intermediate temperature solid oxide fuel cell (IT-SOFC) cathode, due to their excellent oxygen permeation and electrochemical activity towards ORR [5-9]. Recently, Jeen et al. [10] showed that highly oxygen deficient $SrCoO_{3-\delta}$ can act as an "oxygen sponge", which absorb and release oxygen reversibly and in fact promising to design new cathode materials for low temperature SOFCs. Nevertheless, the cubic $SrCoO_{3-\delta}$ phase is chemically unstable and thermally incompatible with yttria-stabilized zirconia (YSZ), gadolinium doped ceria (GDC) and lanthanum strontium gallium magnesium oxide (LSGM) electrolytes. An effective retention method demonstrated so far is cation doping [5-15]. For instance, partial substitution of Co by Fe cation could reduce the temperature expansion coefficient (TEC, α) by reducing the Co content in the structure, which essentially reduces the Co spin state transition (low spin to high spin). Recently, the A-site ordered novel "314-type" cobaltate phase with an idealized chemical composition $Sr_3YCo_4O_{10.5}$ ($Sr_{0.75}Y_{0.25}CoO_{2.625}$) has shown a good potential as cathode for

IT-SOFC (at 800 °C) [16]. This phase is known to form in a tetragonal structure (Space Group (S. G.) *I4/mmm*) having unit cells a = b = $2a_p$ and c = $4a_p$ with a novel oxygen vacancy ordering. The oxygen-vacancies undergoes an order-disorder transition at T_S = 277 °C, and due to the high amount of oxygen vacancies in the oxygen deficient Co-O plane it shows a high O^{2-} ion mobility at higher temperature. Nevertheless, at lower operating temperature (lower than 700 °C) these "314" phases showed very high polarization resistance (R_p) values (for instance for $Sr_{0.7}Y_{0.3}CoO_{2.66}$ R_p = 1 Ω cm^2 at 700 °C [16])

Recently, we have demonstrated the stabilization of "314-type" novel oxygen vacancy ordered phase without A-site ordering [17]. $SrCo_{0.85}Fe_{0.15}O_{2.62}$ is in fact the first example of "314-type" structure in absence of A-site ordering. Due to the availability of high amount of oxygen vacancies in this new phase, we can anticipate a high O^{2-}-ion mobility within the oxygen deficient Co/Fe-O planes, and this would be adequate for the cathode of an IT-SOFC.

Here we report the structure, electrochemical performance and electronic transport properties of a new perovskite related mixed Co-Fe phase with composition $SrCo_{0.85}Fe_{0.15}O_{2.62}$.

2 Experimental Section

2.1 Sample Preparations

The sample was prepared by traditional solid state reaction, starting from stoichiometric amount of $SrCO_3$ (99.9%), Fe_2O_3 (99.99%), Co_3O_4 (99.6%) and were repeatedly ground and heat treated several times before final sintering of pellets at 1,200 °C for 40 hours. The final step was repeated twice.

The performance of $SrCo_{0.85}Fe_{0.15}O_{2.62}$ as an SOFC oxygen electrode was measured on cathode/electrolyte/cathode symmetrical cells. The electrolyte is a Gd-doped ceria $Ce_{0.8}Gd_{0.2}O_{1.9}$ (GDC). A commercial GDC powder (Marion Technologies) was uniaxially pressed at 1 t cm^{-2} and sintered at 1,400 °C for 6 h to produce a 93% dense pellet used as the electrolyte membrane. To prepare the cathodes, an ink was prepared from the $SrCo_{0.85}Fe_{0.15}O_{2.62}$ powder by mixing it with an organic vehicle (terpineol) and a binder (ethyl cellulose). The ink was then screen-printed on both sides of the GDC electrolyte and subsequently sintered at 1,150 °C for 1 h (with a step at 400 °C to remove the organics from the ink), to form porous electrodes with sufficient adherence to the electrolyte.

2.2 Characterization Methods

X-ray powder diffraction (XRD) at room temperature (RT) was performed in a Philips X'Celerator diffractometer (Cu Kα radiation, λ = 1.5406 Å). RT-neutron powder diffraction (NPD) patterns were collected at Paul Scherrer Institute, Switzerland. A wavelength of λ = 1.494 Å was used for the RT-NPD data collection. The high-resolution diffraction patterns were refined with the Rietveld [18] procedure.

The evolution of the oxygen content during the thermal cycling in air was determined in a thermogravimetric analysis (TGA) system. The thermal analysis was carried out over a temperature range of RT–1,000 °C with a heating/cooling rate of 1 °C min^{-1}.

^{57}Fe Mössbauer measurements were performed using a constant acceleration Halder-type spectrometer with a room temperature ^{57}Co source (Rh matrix) in transmission geometry. The velocity scale was calibrated according to the ^{57}Fe Mössbauer spectrum of a pure α-Fe foil recorded at room temperature. The polycrystalline absorbers were prepared in order to contain about 10 mg cm^{-2} of iron and then, to avoid saturation effects. The refinement of Mössbauer hyperfine parameters (δ isomer shift, Δ quadrupole splitting, Γ signal linewidth and relative areas) was performed using both homemade programs and the WinNormos® software.

The electrical conductivity was measured with a standard dc four probe method in the temperature interval RT - 700 °C. The measurement was performed on a sintered pallet (at 1,200 °C for 12 hours) of diameter 7.8 mm and thickness 1.1 mm.

The electrode microstructure was characterized by electron microscopy on a fractured cross-section of the symmetrical cell, with a thermionic gun Jeol JSM 6330F scanning electron microscope, at an acceleration voltage of 15 kV.

The electrochemical performance of the electrodes was characterized by impedance spectroscopy. The symmetrical cells were placed in a furnace between two gold grids for current collection, in a setup described elsewhere [19]. Impedance diagrams were then recorded between 650 °C and 400 °C with a Solartron Modulab frequency response analyzer in the frequency range 1 MHz–100 mHz and an AC signal amplitude of 50 mV. The polarization resistances extracted from the impedance diagrams are multiplied with half the section of the electrodes to account for both electrodes of the symmetrical cell. The good quality of the recorded diagrams was systematically controlled with a Kramer & Kronig test run with an in-house software (CANELEIS®). The impedance diagrams were then fitted by an equivalent circuit using the Zview® software (Scribner Associates Inc).

3 Results and Discussion

3.1 Structural Characterizations

Both the RT-XRD and RT-NPD patterns show extra reflections with respect to oxygen vacancy disordered cubic cell (space group (S.G.): *Pm-3m*). These extra peaks can be indexed on the basis of a tetragonal $2a_p \times 2a_p \times 4a_p$ unit cell (S.G.: *I4/mmm*). Figure 1a shows the final plot of the joint Rietveld refinement of RT-XRD and RT-NPD patterns using the "314-type" structural model ($2a_p \times 2a_p \times 4a_p$, S.G.: *I4/mmm*) for the $SrCo_{0.85}Fe_{0.15}O_{2.62}$ sample. The refinement using the "314-type" structural model shows a nice fitting between the experimental and calculated diffraction patterns, and the extra peaks with respect to the cubic cell are in fact characteristic peaks for the "314-type" structure. The obtained lattice parameters, agreement factors and selected bond lengths and angles, resulting from the joint refinement are given in Table 1.

The crystal structure is shown in Figure 1b. The oxygen atoms (O4) resided on the Co2/Fe2 plane show full occupancy. On the other hand, there are two different crystallographic positions where the oxygen atom could be located in the oxygen deficient layers [(Co1/Fe1–O2, O3)] of the crystal structure, and this layer shows a significant oxygen deficiency. The refinements of the low temperature NPD patterns highlighted a Co^{3+} high spin (HS, $t_{2g}^4e_g^2$) state and intermediate spin (IS, $t_{2g}^5e_g^1$) state ordering (antiferromagnetically aligned) in the oxygen replete layers [17]. Therefore, the oxygen vacancy ordering in the oxygen-deficient Co1/Fe1–O layers and the tilting of octahedra (Co1/Fe1-O1-Co2/Fe2 = 172.9°), due to the Jahn-Teller distortion of the IS Co^{3+} in the oxygen replete region, trigger the quadrupling of the c-axis with respect to the oxygen disordered cubic cell. The high isotropic thermal factors for the O2 and O3 sites (in the oxygen deficient layers, B_{iso} = 2.7 (2) and 3.1 (4) for O2 and O3, respectively) observed in the initial refinement process signal that both these oxygen atoms can be mobile and disordered above room temperature. The exolution and diffusion of these oxygen anions in the oxygen deficient layers is indeed important for both electronic transport and the O^{2-} ion conduction at higher temperature. On the view of high isotropic thermal factors (B_{iso}), we have refined anisotropic displacement factors of the O sites. Figure 2 highlights the crystal structure with anisotropic displacement factors at room temperature. For O4 site, with full occupancy, the thermal ellipsoids are almost spherical. For apical oxygen site (O1 site), with a little oxygen deficiency (occupancy = 0.92 (2)) the thermal ellipsoids are oriented along 110 direction. Nevertheless, for O2 and O3 sites, where most of the oxygen deficiency is observed, the anisotropy of the thermal ellipsoids is clear, with the largest thermal motions perpendicular to the Co/Fe−O bonds, as expected. As mentioned earlier, it is obvious that this different oxygen arrangement in successive Co/Fe–O layers is the driving force for the observed tetragonal superstructure.

To reveal the thermal evolution of the loosely bounded oxygen anions in the oxygen deficient Co1/Fe1 layers, we have measured the TGA upon thermal cycling between RT to 1,000 °C. As shown in the Figure 3, the weight of the sample is constant up to 400 °C and the oxygen exolution starts above that temperature. At 650 °C, which is the highest temperature for electrochemical performance measurements in the present study, the sample shows weight loss of 0.8%. This weight loss is equivalent to the loss of 0.09 of the total oxygen content, and in fact corresponds to the ∼13% of the total O2 and O3 atoms. This indeed points out that most of the mobile oxygen anions are still present at this temperature. However, above 700 °C the total oxygen content goes below 2.5. The linear thermal expansion coefficient (TEC) obtained from the high temperature XRD patterns for a similar "314-

type" compound with composition $SrCo_{0.75}Fe_{0.25}O_{2.64}$ (S1 in the supporting information, see also [17]) is $\alpha \sim 19 \times 10^{-6}$ K^{-1}. Therefore we can expect the similar TEC value for the present material, and this is comparable to other cobalt-containing perovskites [14-16].

3.2 Mössbauer Spectroscopy

The room temperature ^{57}Fe Mössbauer spectrum is shown in Figure 4 and the refined hyperfine parameters are summarized in Table 2. The spectrum presents two paramagnetic components with isomer shifts δ (Fe1) = –0.021 mm s^{-1} and δ (Fe2) = 0.245 mm s^{-1}. Each component was actually calculated considering a distribution of the quadrupole splitting parameter (Δ), *i.e.*, as the sum of quadrupole doublets with Lorentzian shape, same isomer shift and different quadrupole splitting values (see inset of Figure 4). These distributions may be related to cationic (Fe, Co) disorder around iron atoms. The values of hyperfine parameters of the Fe2 and Fe1 components (Table 2) are consistent with high spin Fe^{4+} ions in octahedral sites and four- or five-fold coordinated high spin Fe^{3+}, respectively. Furthermore, the shape of the quadrupole splitting distributions may reflect some heterogeneities in the Fe environment, *i.e.*, site distortions and/or occurrence of oxygen vacancies in the first coordination sphere of iron ions, particularly for the Fe 1 signal.

As expected, heterogeneous oxidation states distribution is found when the Mossbauer spectroscopy is combined with the joint RT-NPD and RT-XRD analysis, giving the following chemical formula: $Sr(Co^{4+}_{0.19}Co^{3+}_{0.81})_{0.85}(Fe^{4+}_{0.5}Fe^{3+}_{0.5})_{0.15}O_{2.62\pm0.02}$.

3.3 Electrical Transport Properties

Figure 5a shows the temperature dependence of electrical conductivity (σ (T)) measured on a sintered pellet over a temperature range of 100 °C to 700 °C. It shows a semiconducting behavior up to 200 °C, then exhibits a much weaker temperature dependence and becomes metallic like above 450 °C. At 600 °C, σ (T) exhibits a value around 200 S cm^{-1}. Such a value of electrical conductivity satisfies the requirement for the cathode material for SOFC at that temperature. The Arrhenius plot (ln σT *vs*. T^{-1}), shown in Figure 5b displays a nonlinear variation with the temperature, and could be due to the change in the amount of electronic charge carriers with temperature. A linear like dependence of ln σT *vs*. T^{-1} observed at RT - 400 °C range, and this could be due to the small polaron conduction. The polaronic mechanism in electrical conductivity is due to the presence of Co^{4+} and Fe^{3+} in the structure, as observed from the RT Mössbauer spectroscopy data. However, above 400 °C the material gradually loose oxygen (see Figure 3), and in fact changes the total amount of Co^{4+} (and/or Fe^{4+}) in the structure. Therefore, the decreasing conductivity behavior above 400 °C could be attributed to the decrease in the amount of electronic charge carriers due to the gradual change of the oxygen content rather than of oxygen (O2 and O3) disorder in the oxygen deficient Co1/Fe1-O layers with increasing temperature.

3.4 SOFC Oxygen Electrode Performance

The previous parts suggest that $SrCo_{0.85}Fe_{0.15}O_{2.62}$ could be a good oxygen electrode: the electronic conductivity is high, the high amount of oxygen vacancies suggests a good oxide ion mobility, and the mixed valence Co and Fe suggests catalytic properties. Then, its performance as an SOFC oxygen electrode is characterized. Figure 6a shows a typical impedance diagram recorded on the $SrCo_{0.85}Fe_{0.15}O_{2.62}$/GDC/$SrCo_{0.85}Fe_{0.15}O_{2.62}$ symmetrical cell, at 600 °C. Impedance diagrams were fitted with an equivalent circuit made of a simple series resistance to model the ohmic loss in the electrolyte, and two R-CPE circuits to account for the electrode processes. The polarization resistance of the electrode is the sum of the resistances of these two contributions, and its evolution as a function of temperature is represented on Figure 6b. The polarization resistance of such an electrode is very low on the whole temperature range, reaching R_p = 0.1 Ω cm^2 at a temperature as low as 600 °C, demonstrating the high electrocatalytic activity of $SrCo_{0.85}Fe_{0.15}O_{2.62}$. As a comparison Szasz et al. [20] reached only R_p = 0.2 Ω cm^2 at the same temperature for a $La_{0.6}Sr_{0.4}Co_{0.2}Fe_{0.8}O_{3-\delta}$ (LSCF) electrode on a thoroughly optimized YSZ/GDC/LSCF electrode architecture, which is twice the value measured in this study. Moreover, the electrode was prepared starting from a powder synthesized by a solid-state route, usually leading to a coarse microstructure. Indeed, the scanning electron microscope (SEM) picture of the electrode cross-section (Figure 7) shows the coarse microstructure of the electrode, with average grain size of around 5–10 µm, which is far higher than typical submicronic grain usually obtained in optimized electrodes. The electrode microstructure plays an essential role on the electrode performance, especially its specific

area. Decreasing the average grain size of the starting powder by changing the synthesis route could lead to an increase of the specific area of the electrode, and thus a further decrease of its polarization resistance, resulting in super-effective oxygen electrodes.

4 Conclusions

A new perovskite material, $SrCo_{0.85}Fe_{0.15}O_{2.62}$ with "314-type" oxygen vacancy ordered structure, in fact the first "314-phase" without A-site ordering has been prepared and studied as a cathode for IT-SOFC. The combination of RT-XRD and RT-NPD patterns are employed to determine the crystal structure, and shows the formation of "314-type" oxygen-vacancy ordered structure with $2a_p \times 2a_p \times 4a_p$ unit cell. The structure contains alternate (001) planes of Co2/Fe2-O octahedral and Co1/Fe1-O planes containing 4 and 5 coordinated Co and Fe. The RT Mössbauer spectroscopy measurement and the joint refinement of RT-XRD and RT-NPD confirm the presence of mixed valence states (3+ and 4+) for both Fe and Co. The electrical conductivity at 600 °C is sufficient ($\sigma_{(600\,°C)}$ = 200 S cm^{-1}) to act as a cathode material. At 600 °C, the polarization resistance is as low as R_p = 0.1 Ω cm^2, which is comparable with the values obtained at this temperature for best SOFC cathode materials. All these results demonstrate that at 600 °C, this new material is a MIEC exhibiting excellent activity for the ORR, and this makes it a promising cathode material for an IT-SOFC. We would like to emphasize that the improvement in the electrode microstructure could enhance the cathode properties of this new material.

Acknowledgements

The authors are indebted to the CNRS, Université Bordeaux and SOPRANO project (Seventh Framework Programme FP7/2007–2013 under Grant Agreement no. 214040) for funding this work. This work is based on experiments performed at the Swiss spallation neutron source SINQ, Paul Scherrer Institute, Villigen, Switzerland. Authors also wish to thank Dr. Vladimir Pomjakushin for his help in collecting the neutron powder diffraction patterns. The authors also thank Dr. Jean-Claude Grenier and Dr. Aline Rougier for fruitful discussions.

References

1. B. Steele , A. Heinzel , Nature 2001, 414, 345.
2. H. Bouwmeester , H. Kruidhof , A. Burggraaf , Solid State Ionics 1994, 72 (PART 2), 185.
3. E. Perry Murray , S. Barnett , Solid State Ionics 2001, 143, 265.
4. C. Sun , R. Hui , J. Roller , Journal of Solid State Electrochemistry 2010, 14, 1125.
5. Z. Shao , S. Halle , Nature 2004, 431, 170.
6. J. Peña-Martínez a, D. Marrero-López , J. C. Ruiz-Morales , B. E. Buergler , P. Núñez , L. J. Gauckler , Solid State Ionics 2006, 177, 2143.
7. A. Tarancón , S. J. Skinner , R. J. Chater , F. Hernández-Ramírez a, J. A. Kilnerb , Journal of Materials Chemistry 2007, 17, 3175.
8. J.-H. Kim , A. Manthiram , Journal of the Electrochemical Society 2008, 155, B385.
9. J. Stevenson , T. Armstrong , R. Carneim , L. Pederson , W. Weber , Journal of the Electrochemical Society 1996, 143, 2722.
10. H. Jeen , W. Choi , M. Biegalski , C. Folkman , I.-C. Tung , D. Fong , J. Freeland , D. Shin , H. Ohta , M. Chisholm , H. Lee , Nature Materials 2013, 12, 1057.
11. K. Zhang , R. Ran , L. Ge , Z. Shao , W. Jin , N. Xu , Journal of Membrane Science 2008, 323, 436.
12. F. Wang , Q. Zhou , T. He , G. Li , H. Ding , Journal of Power Sources 2010, 195, 3772.
13. W. Zhou , Z. Shao , R. Ran , R. Cai , Electrochemistry Communications 2008, 10, 1647.
14. A. Aguadero , D. Pérez-Coll , J. Alonso , S. Skinner , J. Kilner , Chemistry of Materials 2012, 24, 2655.
15. W. Yang , H. Zhang , C. Sun , L. Liu , J. Alonso , M. Fernández-Díaz , L. Chen , Inorganic Chemistry 2015, 54, 3477.
16. Y. Li , Y. Kim , J. Cheng , J. Alonso , Z. Hu , Y.-Y. Chin , T. Takami , M. Fernández-Díaz , H.-J. Lin , C.-T. Chen , L. Tjeng , A. Manthiram , J. Goodenough , Chemistry of Materials 2011, 23, 5037.
17. S. Marik , M. Chennabasappa , J. Fernández-Sanjulián , E. Petit , O. Toulemonde , Inorganic Chemistry 2016, 55, 9778.
18. J. Rodriguez-Carvajal, An introduction to the program FULLPROF, Laboratoire Leon Brillouin (Saclay: CEA-CNRS), Saclay, France, 2001.
19. A. Flura , C. Nicollet , S. Fourcade , V. Vibhu , A. Rougier , J.-M. Bassat , J.-C. Grenier , Electrochimica Acta 2015, 174, 1030.
20. J. Szasz , F. Wankmüller , V. Wilde , H. Störmer , D. Gerthsen , N. Menzler , E. Ivers-Tiffée , ECS Transactions 2015, 66, 79.

Table 1 Refined crystallographic parameters and reliability factors obtained from Rietveld analysis (using joint RT-NPD and RT-XRD patterns) for the $SrCo_{0.85}Fe_{0.15}O_{2.62}$ sample.

Atomic coordinates – Space Group: *I4/mmm* (139)						
Atom	Wyck.	x	y	z	Occup.	B_{iso} / Å^2
Sr1	4e	0	0	0.1270(8)	1	0.9(1)
Sr2	4e	0	0	0.6349(7)	1	0.7(1)
Sr3	8g	0	1/2	0.1313(6)	1	0.8(1)
Co1	8h	0.2486(6)	0.2486(6)	0	0.88(2)	0.2(1)
Fe1	8h	0.2486(6)	0.2486(6)	0	0.12(2)	0.2(1)
Co2	8f	1/4	1/4	1/4	0.84(2)	0.2(1)
Fe2	8f	1/4	1/4	1/4	0.16(2)	0.2(1)
O1[a]	16m	0.260(1)	0.260(1)	0.1176(3)	0.92(2)	1.6(1)
O2[b]	8i	0.284(1)	0	0	0.46(2)	2.7(2)
O3[c]	8j	0.738(3)	1/2	0	0.24(1)	3.1(4)
O4[d]	16n	0	0.250(1)	0.245(1)	1	0.9(1)

Cell parameters				Total oxygen content
a / Å	b / Å	c / Å	V / Å^3	2.62(2)
7.7275(1)	7.7275(1)	15.4716(2)	923.87(4)	

Reliability factors Rp = 0.0402 Rwp = 0.0547 RF = 0.0557 χ^2 = 2.64

Anisotropic thermal factors: [a]$\beta_{11} = \beta_{22} = 0.028(3)$, $\beta_{33} = 0.014(2)$; $\beta_{12} = \beta_{13} = \beta_{23} = 0$; [b]$\beta_{11} = 0.06(1)$, $\beta_{22} = 0.016(6)$, $\beta_{33} = 0.026(6)$; $\beta_{12} = \beta_{13} = \beta_{23} = 0$; [c]$\beta_{11} = 0.05(2)$, $\beta_{22} = 0.03(2)$, $\beta_{33} = 0.08(2)$; $\beta_{12} = \beta_{13} = \beta_{23} = 0$; [d]$\beta_{11} = 0.011(2)$, $\beta_{22} = 0.01(1)$, $\beta_{33} = 0.013(2)$; $\beta_{12} = \beta_{13} = \beta_{23} = 0$

Table 2 ^{57}Fe Mössbauer hyperfine parameters extracted from the analysis of the $SrCo_{0.85}Fe_{0.15}O_{2.62}$ room temperature spectrum (Fig. 3). δ: isomer shift (related to α-Fe at room temperature), $<\Delta>$: mean value of the quadrupole splitting distribution and Γ: Lorentzian linewidth.

Signal	δ / mm s^{-1}	$<\Delta>$ / mm s^{-1}	Γ / mm s^{-1}	Area / %	Assignment
Fe1	0.245 (2)	0.39	0.32 (–)	50(2)	Fe^{3+} [Td] or 5-fold coord.
Fe2	–0.021 (2)	0.42	0.30 (–)	50(2)	Fe^{4+} [Oh]

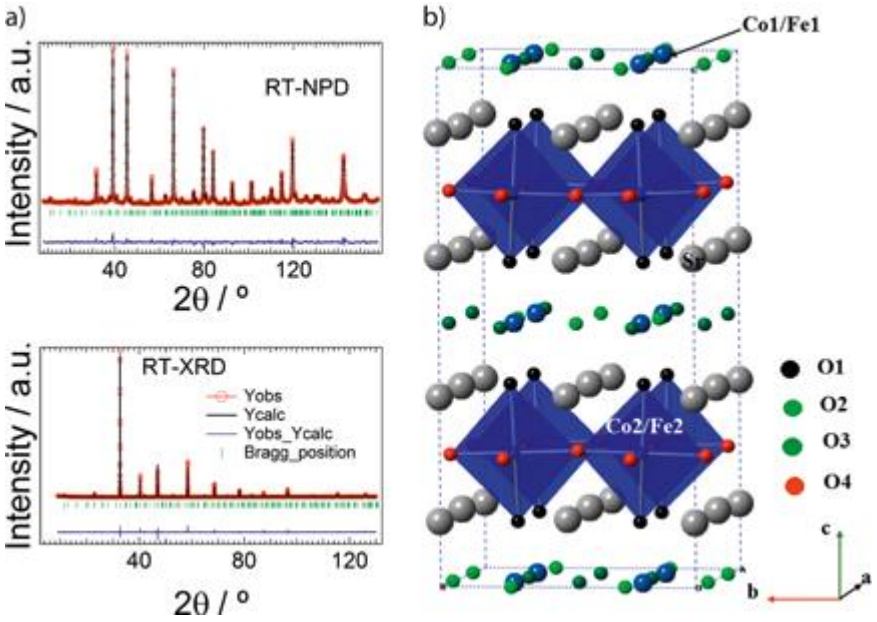

Figure 1. - (a) Final observed, calculated, and difference profiles (tetragonal, I4/mmm, *$2a_p \times 2a_p \times 4a_p$ type unit cell) of the RT-NPD and RT-XRD joint refinement for the $SrCo_{0.85}Fe_{0.15}O_{2.62\pm0.02}$; (b) Crystal structure of the same material. The refinement shows that the Co1/Fe1 sites are surrounded by oxygen vacancies, whereas the Co2/Fe2 sites are oxygen replete.*

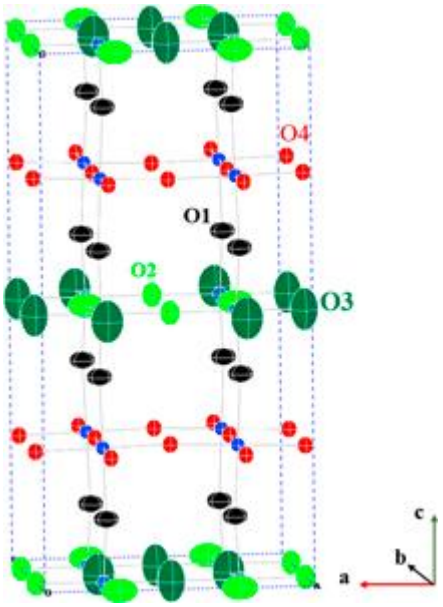

Figure 2. - Tetragonal crystal structure highlighting the orientations of the oxygen ellipsoids (anisotropic thermal factors, 80% of probability) at room temperature for the $SrCo_{0.85}Fe_{0.15}O_{2.62\pm0.02}$ material.

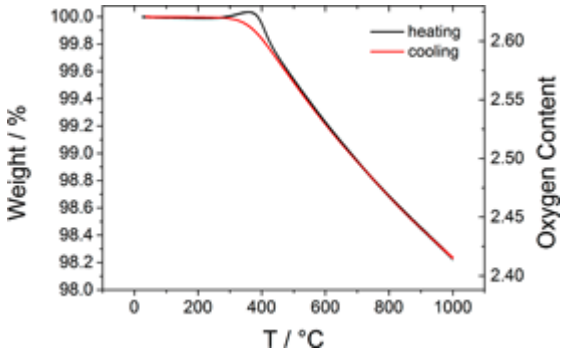

Figure 3. - Thermogravimetric analysis (TGA) curves and the corresponding oxygen content for the oxygen deficient $SrCo_{0.85}Fe_{0.15}O_{2.62\pm0.02}$ measured upon heating up and cooling down between RT and 1,000 °C in air.

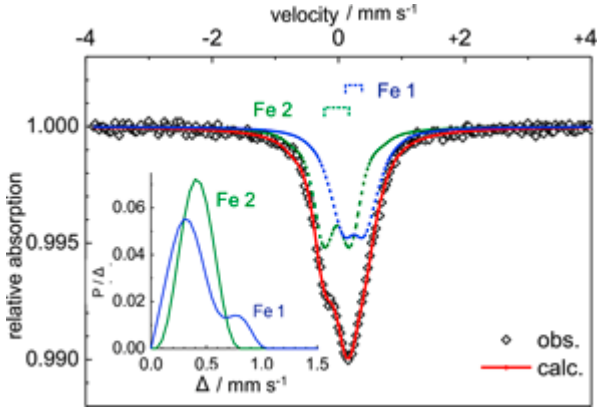

Figure 4. - Room temperature ^{57}Fe Mössbauer spectrum of the $SrCo_{0.85}Fe_{0.15}O_{2.62\pm0.02}$ sample. The experimental spectrum (dotted line) was reconstructed considering two components (dashed lines) with distributions of the quadrupole splitting (Δ) values (inset). Associated hyperfine parameters are reported in Table 2.

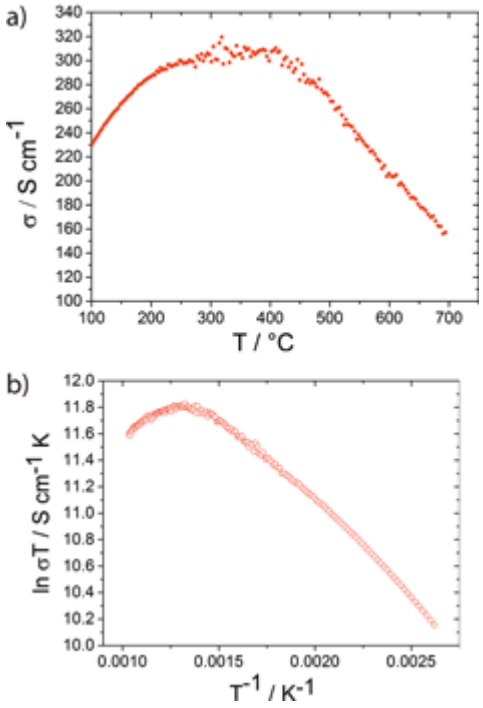

Figure 5. - (a) Temperature dependence of the electrical conductivity (σ (T)); (b) Arrhenius plot, ln σT vs. T^{-1}, for the oxygen deficient $SrCo_{0.85}Fe_{0.15}O_{2.62\pm0.02}$ sample measured in air.

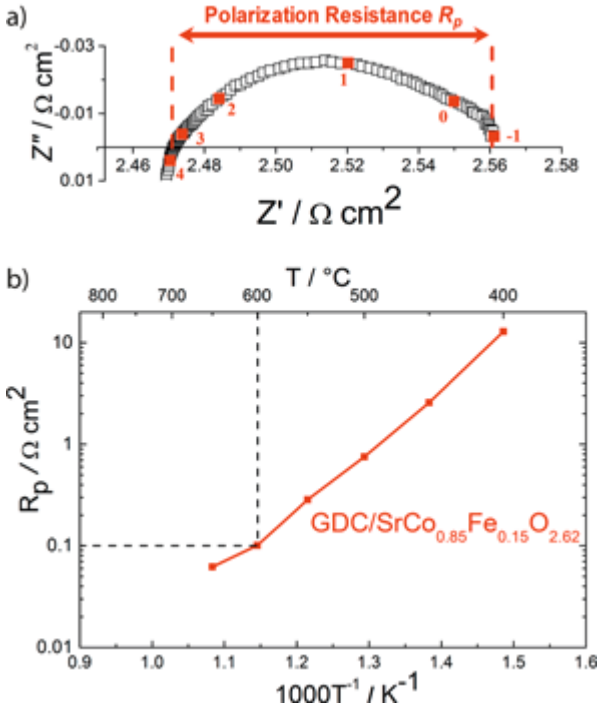

Figure 6. - (a) Typical impedance spectra recorded on the $SrCo_{0.85}Fe_{0.15}O_{2.62}$/GDC/$SrCo_{0.85}Fe_{0.15}O_{2.62}$ symmetrical cell, at 600 °C (numbers are frequency decades); (b) Temperature dependence of the polarization resistance (R_p). It shows that the R_p = 0.1 Ω cm² at a temperature as low as 600 °C, interpreting the high electro-catalytic activity of $SrCo_{0.85}Fe_{0.15}O_{2.62\pm0.02}$.

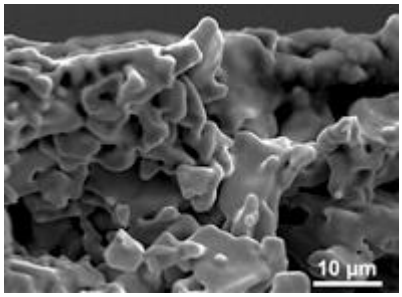

Figure 7. - The scanning electron microscope (SEM) picture of the $SrCo_{0.85}Fe_{0.15}O_{2.62\pm0.02}$ electrode cross-section.